

1 This manuscript is a EarthArxiv preprint and has been submitted for publication in MARINE AND
2 PETROLEUM GEOLOGY. Please note that the manuscript has not been peer-reviewed yet and that late
3 versions of the manuscript may change due to the review process. If accepted, the final version of the
4 manuscript will be available via the 'Peer-reviewed Publication DOI' link on the right-hand side
5 of this page.

6

7 **Gas - escape features along the Trzebiatów Fault offshore Poland: evidence for a leaking petroleum**
8 **system**

9 Quang Nguyen^{1*}, Michal Malinowski^{1,2}, Regina Kramarska³, Dorota Kaulbarsz³, Leslaw Mil³, Christian Hübscher⁴

10 ¹ Institute of Geophysics, Polish Academy of Sciences, Warsaw

11 ² Geological Survey of Finland, Espoo

12 ³ Polish Geological Institute – National Research Institute, Maritime Geology branch, Gdańsk

13 ⁴ Institute of Geophysics, University of Hamburg, Hamburg

14 **Abstract:** New 2D high resolution seismic and hydro-acoustic data demonstrate the presence of methane
15 in the shallow sediments and its origin in the Pomeranian Bight, southern of the Baltic Sea area. Various
16 shallow gas features were identified in the Gryfice block, along the inverted Trzebiatów fault zone,
17 including chimneys, bright spots, acoustic blanking, pockmarks, and polarity reversal. Structural and
18 stratigraphic interpretation with support of seismic attributes was carried out to show the potential of fluid
19 migration pathways from the Upper Triassic formation reservoirs to shallow sediments below seabed and
20 helps in explanation of how this natural gas escapes to the sea bottom. Amplitude-vs-offset (AVO) analysis
21 verified remnants of free gas existence in the Upper Triassic potential reservoir and helped locating free
22 gas deposits within sediments. Hydro-acoustic data illustrated the gas chimneys' anomalies and
23 corresponding free gas accumulation in Pleistocene to Quaternary successions. Leaking of gas to sea surface
24 was also proved by exposure of pockmarks on multibeam (bathymetry) data. We combine seismic, hydro-
25 acoustic data and information on petroleum system from previous studies to explain signatures of free gas
26 and its migration from lower reservoirs to shallow sediments.

27 **Keywords:** reflection seismic, hydro-acoustics, fluid escape, shallow gas, petroleum system

28 **1. Introduction**

29 Methane (CH₄) is the most abundant gas accumulated in shallow sediments compared to carbon dioxide,
30 hydrogen sulfide, and higher chain hydrocarbon. Gas (hydrocarbons in general) can originate from either
31 biological or thermogenic processes. While the biogenic gas is generated by bacterial activity mainly within
32 few meters of sediments (Parkes et al, 1990), the thermogenic gas is derived from organic materials at high
33 pressures and temperatures and frequently at depth of more than 1000 m (Floodgate and Judd, 1992).

* Corresponding author. Institute of Geophysics, Polish Academy of Sciences, Warsaw, Poland.
Email address: qnguyen@igf.edu.pl (Quang Nguyen)

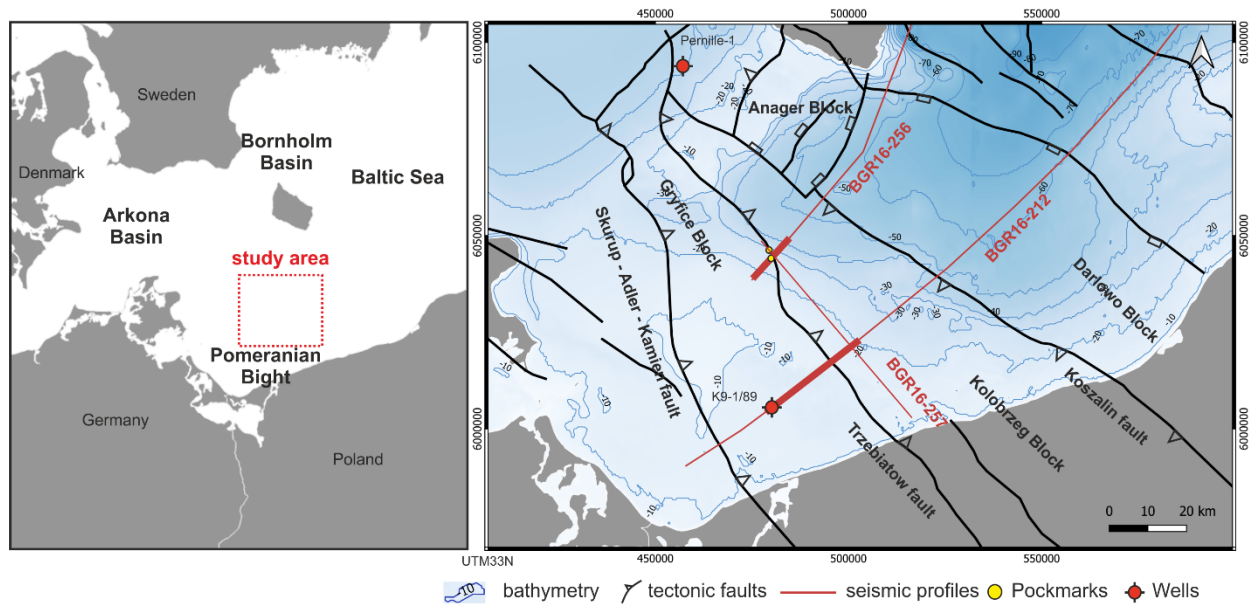
34 Thermogenic gas often migrates to the surface and is being trapped in shallow sediments. Presence of
35 shallow gas impacts both the geosystem and various ecosystems: e.g., geohazards related to stability of the
36 offshore infrastructure (Fleischer et al., 2001; Hovland et al., 1993; Naudts et al., 2009) or drilling offshore
37 oil and gas wells (Adams and Kuhlman, 1991; Schroot and Schüttenhelm, 2003; Ren et al., 2019), as well
38 as water chemistry and flora and fauna habitats (Idczak et al. 2020; Judd and Hovland, 2009).

39 Free gas presence in shallow marine sediments can be recognized in seismic and hydro-acoustic data by
40 some distinct signal appearance. Acoustic turbidity or acoustic blanking are seismic frequency related
41 features due to scattering and absorption of seismic energy in gas charged areas (Hovland and Judd, 1988).
42 While acoustic turbidity appears as chaotic reflections, being mostly found in pockmark areas, acoustic
43 blanking represents absence of reflections beneath gassy layers (Mathys et al., 2005; Tóth et al., 2014). The
44 acoustic blanking is one of the most common gas-related features, it appears as smear zone where
45 reflections are faint and absent in certain level (Judd and Hovland, 2009; Schroot et al., 2005). This may
46 result of migration of free gas or reflection of acoustic energy by overlapping hard sediment (Judd and
47 Hovland, 1992). Gas accumulation areas can also cause amplitude bright spots which usually occur at depth
48 of more than 100 m and possibly at relatively high pressure (Hovland and Judd, 1988). Bright reflectivity
49 zones often form reverberations or ringing in acoustic data (Davy, 1992; Tóth et al., 2014). They are similar
50 to bright spots, but occur in shallower records. These features are frequently observed together with acoustic
51 turbidity zones (Judd and Hovland, 1992). Decrease of seismic velocity and lower density in gas-charged
52 sediments can also cause polarity reversal of the corresponding reflections (Garcia-Gil et al., 2002; Kim,
53 2020).

54 Presence of gas in the shallow sediments in the Baltic Sea area was investigated in many studies using
55 either seismic or hydro-acoustic data. Blanking and turbidity evidence of gas bubbles were found in
56 organic-rich near surface sediments in Arkona Basin (Mathys et al., 2005; Thießen et al., 2006) and in
57 Eckernförde Bay (Abegg and Anderson, 1997). Shallow gas distribution in Holocene marine mud was
58 mapped in Aarhus Bay and Skagerrak (Jensen and Bennike, 2009; Laier and Jensen, 2007). Free gas in
59 Holocene mud was also detected in the Bornholm Basin (Laier and Jensen, 2007; Tóth et al., 2014).
60 Offshore Poland, studies on shallow gas were conducted since the early 90s (Jaśniewicz et al., 2019).
61 Majority of the studies focused on the eastern and central part of the Polish Exclusive Economic Zone
62 (EEZ) especially in the Gdansk Basin and the Słupsk Furrow (Jakacki et al., 2002; Tęgowski et al., 2003;
63 Brodecka et al., 2013; Jørgensen and Fossing, 2012; Majewski and Klusek 2011, 2014; Idczak et al. 2020).
64 Geochemical studies performed by the consortium led by the Polish Geological Institute in 2005-2008
65 indicated occurrence of thermogenic gas in near seabed waters (Jaworowski et al. 2010; Wagner, 2011). It
66 was linked with the Paleozoic petroleum system, with active oil and gas production in the eastern part of

67 the EEZ (Jaworowski et al. 2010). The area of Pomeranian Bight in the western part of the EEZ is less
68 studied with the acoustic data collected during 1970s and 1980s (Jaśniewicz et al., 2019).

69 In this study, we analyze multichannel reflection seismic (MCS), high-frequency hydro-acoustic
70 (parametric sub-bottom profiler) and bathymetric (multibeam) data acquired in the greater Pomeranian
71 Bight area, southern Baltic Sea during RV Maria S. Merian research cruise MSM52 in 2016 (Hübscher et
72 al., 2017). The study area is located at the offshore extension of the established Paleozoic (mostly
73 Carboniferous) and Permian (both Zechstein and Rotliegend) petroleum play (Karnkowski et al., 2010).
74 Our data provide evidence for gas presence in the shallow sediments, as well as its link with the deeper
75 geological structure (Trzebiatów Fault). Amplitude-versus-offset (AVO) analysis of seismic data confirms
76 the presence of gas at the deeper reservoir level, while seismic data portrays gas migration pathways (gas
77 chimneys).



78
79 **Figure 1.** Location of the study area (greater Pomeranian Bight, Baltic Sea). Location of the seismic lines
80 used in this study at bathymetry map with main tectonic structures overlaid (modified from Janik et al.,
81 2022). Part of the seismic sections showing shallow gas features are highlighted by a thick red line. Yellow
82 dots show two pockmarks' locations identified by multibeam data.

83

84 2. Geological background

85 2.1. Sub-Quaternary geology

86 The study area is located offshore Poland within area of Gryfice block, in the inverted part of the Permian
87 - Mesozoic Polish Basin, so called Mid - Polish Swell (Dadlez, 2003; Krzywiec, 2006). There are two main
88 inversion-related fault zones: Adler-Kamień and Trzebiatów faults, rooted in the pre-Permian basement
89 (Figure 1).

90 Development of the Permian - Mesozoic basin and its sediments distribution are consequences of two
91 tectonic regimes: basin extension commenced in the Rotliegend through Mesozoic to Lower Cretaceous
92 and later inversion tectonism in Late Cretaceous period (Vejbaek et al., 1994; Krzywiec, 2006, 2022).
93 Dominant fault systems in the north western part of Mid-Polish Trough (MPT) are NW-SE trending
94 (Scheck-Wenderoth and Lamarche, 2005). During extensional basin subsidence stage, sediments and
95 structural features of the MPT were controlled by deep-seated and listric normal faults. These faults systems
96 were then strongly reactivated in the basin inversion stage and extended from the basement upward into
97 Mesozoic series (Vejbaek et al., 1994; Schlüter et al., 1997; Krzywiec, 2006), the Trzebiatów fault zone
98 crossing our study area (Figure 1) is one of such faults. The Trzebiatów fault zone in the NE of the section
99 (Figure 3) is a typical extension fault system inverted in a compressional tectonic regime (Schlüter et al.,
100 1997; Krzywiec, 2002), this fault zone roots within pre-Zechstein and accompanied by asymmetric fault-
101 propagation folds developed within the Mesozoic sedimentation.

102 Mesozoic sediments were studied by several authors (e.g., Dadlez, 1978, 1980, 2002, 2003; Krzywiec,
103 2006; Zimmermann et al., 2015). Lower Triassic deposits offshore Pomeranian Bight are represented by
104 red-bed sediments of fine grain sandstones, silt and shale (Erlstrom et al., 1997). While carbonate-
105 evaporites are dominant in Middle Triassic, the red-bed clastics come back in the Upper Triassic (Dadlez
106 et al., 1995). Lithology from nearby wells data (Pernille-1 unpublished well report, 1989) also reveals a
107 thin layer of claystones by the end of Keuper, forming a potential seal in petroleum play of the study area.
108 Sediment deposits are consistent during Lower and Middle epoch of Jurassic. The lithology is
109 predominantly clay with interbedded interlaminated fine grain sand. The Upper Jurassic has the same
110 lithology as Lower and Middle Jurassic, but it is eroded in some areas due to strongly reverse faulting
111 during inversion, similarly to the Lower Cretaceous deposits. Sedimentation of the Upper Cretaceous
112 develops to the Maastrichtian in the southwest and until Early Paleogene in the northeast of the basin.
113 Marginal marine limestone is dominant lithology of this formation. In this study, we consider the Upper
114 Triassic succession as potential reservoir rocks (Figure 2, see section 2.3 below).

115

116 *2.2. Quaternary geology*

117 In the area of the Trzebiatów Fault zone offshore Poland, Tertiary sediments are almost absent due to
118 erosion during Late Cretaceous - Paleogene inversion (Krzywiec, 2003, 2006), the Mesozoic formations
119 are the direct substrate of the Quaternary sediments. The total thickness of the Quaternary formations in
120 this region is estimated at about 30 - 40 m (Kramarska et al., 1999). The Quaternary profile in the south-
121 eastern part of the Gryfice block is represented by the two levels of Pleistocene glacial tills, separated by
122 series of fluvio-glacial sands and gravels (Kramarska, 1998). The thickness of the lower till layer is
123 estimated to be several meters, in some places it can reach about 10 m. The layer of the upper till is thinner,
124 often topped with lacustrine sands, silts and gyttas, locally organic silts and peat. These types of sediments
125 can be found in many places in the Gryfice block. Numerous radiocarbon dates of organic sediments
126 indicate that lake accumulation took place mainly in the early Holocene (e.g., Kramarska, 1998). The sea
127 bottom surface is covered with a layer of fine-grained sands deposited in the Littorina and Post-Littorina
128 sea, from the middle Holocene to the present day.

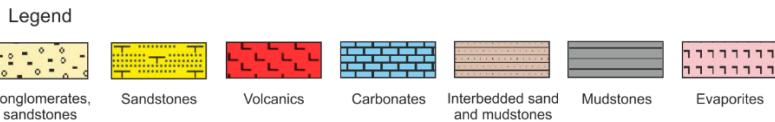
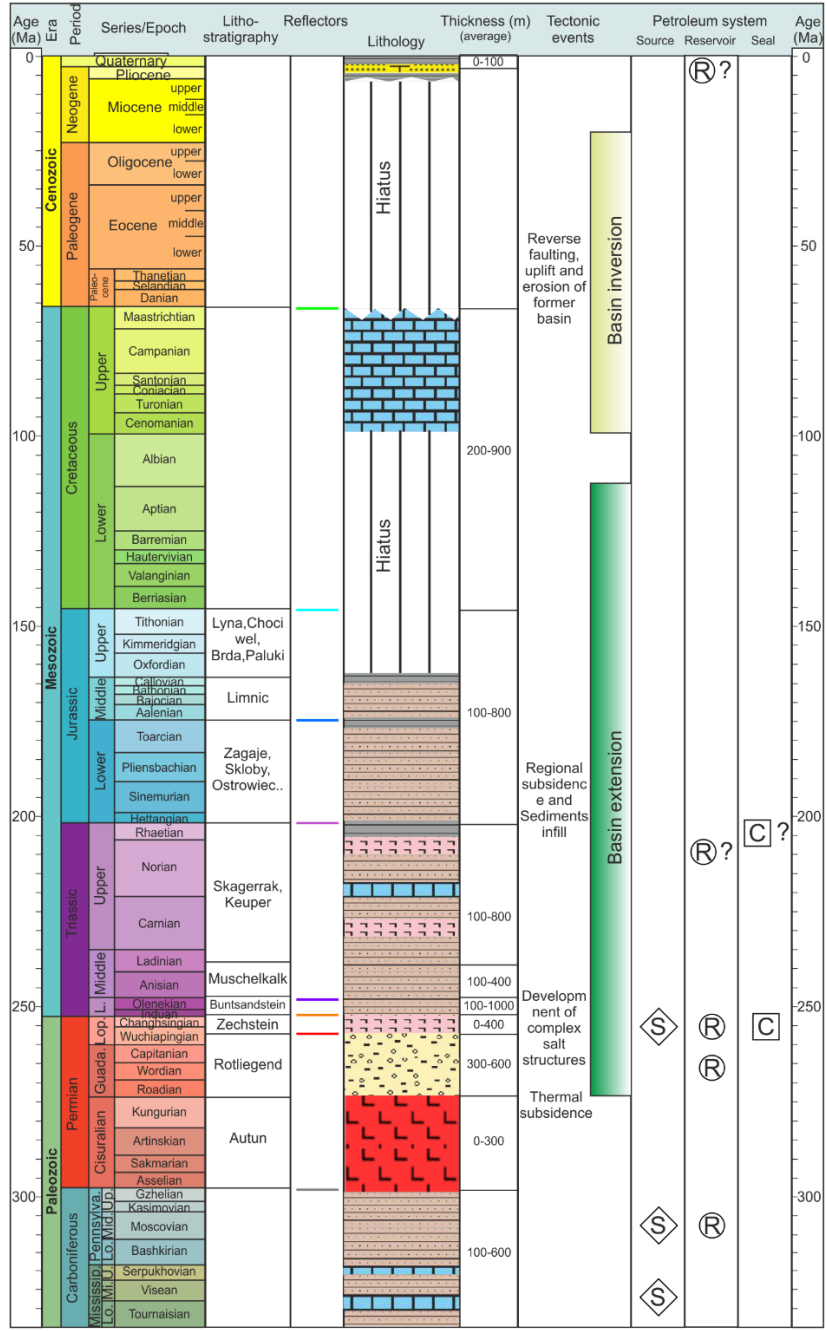
129 The Pleistocene sandy sediments are dominant in the north-western section of the Gryfice block. This
130 sedimentary series lays directly on top of the older glacial till (the younger till is not present). The lower
131 part of sandy layer is most probably represented by fluvio-glacial sands and gravels. The upper part is a
132 continuation of the river and lake sediments accumulated during the warming period MIS3
133 (interplenivistulian). The sediments identified in cores (Kramarska, 1998) are represented by sands and silty
134 sands with plant detritus and pieces of wood, dated with C14 at about 45-22 ka BP. The surficial part of the
135 sand layer, with a thickness less than the resolution of the wave image, represents the marine environment
136 of the younger Holocene.

137 *2.3. Petroleum system of Western Pomerania*

138 Petroleum system of Western Pomerania, encompassing both the onshore and offshore part of Poland
139 extending to the eastern part of the Northeast German Basin, is specifically described in numerous studies
140 (Karnkowski et al., 2010; Kotarba et al., 2004; Gawenda 2011). Lithostratigraphic chart of petroleum
141 system offshore Poland (Figure 2) is built based on nearby well stratigraphy data (Erlstrom et al., 1997;
142 Pernille-1 unpublished well report, 1989). Source rocks in the Western Pomerania are divided into two
143 main units: the older Carboniferous deposits comprised of Tournaisian mudstones and claystones and the
144 younger Zechstein Main Dolomite. Geochemical modeling of onshore Polish wells shows that both the
145 Carboniferous source rock and Main Dolomite (Zechstein) display poor to fair source potential, and locally
146 very good to excellent oil-source potential. The generation of hydrocarbons of both source rock types begins
147 in the time span between the Middle Triassic and Late Jurassic (Kosakowski et al., 2006). Major recognized

148 reservoir rocks are either Carboniferous or Rotliegend clastics, sealed by Zechstein evaporates (Karnkowski
149 et al., 2010). Grainstones and packstones within the Main Dolomite (Zechstein) unit (Karnkowski et al.,
150 2010) are forming the third reservoir level. Zechstein formation can be considered as a closed hydrocarbon
151 play, where source, reservoir and seal rocks are in the same location.

152 Offshore West Pomerania is considered as a poor oil and gas production area even though numerous
153 boreholes were drilled (Karnkowski et al., 2010), most of proven hydrocarbon fields locate onshore
154 Pomerania in the North East German – Poland Basin (Kraus et al., 2018). The Lower Permian (Rotliegend)
155 sandstones and Upper Permian (Zechstein) carbonates are dominant as main hydrocarbons reservoirs in the
156 region, proven by numerous wells (Gawenda, 2011). Mesozoic sediments were targets of many exploration
157 offshore wells to test hydrocarbon prospects in the surrounding area of the offshore West Pomerania such
158 as Arkona Basin, Western of Bornholm island (Kraus et al., 2018). Reservoir rocks of Mesozoic sediments
159 were Lower Jurassic sandstones from Roone and Hasle formation, Upper Triassic Keuper sandstone from
160 Skagerrad formation and Lower Triassic sandstone from Buntsandstein formation. These sandstones
161 generally consist of fine to medium grained, moderately to well sorted minerals deposited in fluvial
162 environment. Although the Lower Jurassic and Lower Triassic sandstones (expected reservoirs) were very
163 good to excellent in term of porosity and thickness proven by well data (e.g., Pernille-1, Stina-1 unpublished
164 well report, 1989), however, there was no clearly show of hydrocarbon accumulation in Mesozoic strata.
165 This may due to reservoir rocks located in the transition (oil-gas) zone of hydrocarbon generation
166 (Karnkowski, 2010) or absence of good charge and seal condition (Bachmann et al., 2010). Apart from
167 petroleum, the Mesozoic sandstones in the West Pomerania were analyzed as a significant potential of
168 geothermal heating and aquifer thermal energy storage in recent years (Kilhams et al., 2018; Frick et al.,
169 2022).



170

171 **Figure 2.** Simplified lithostratigraphy and petroleum system of West Pomeranian, offshore Poland. The
 172 graph is based on well stratigraphy, tectonics, and lithology from Erlstrom et al. (1997) and Pernille-1
 173 unpublished well report (1989).

174

175 **3. Data and methods**

176 Reflection seismic, hydro-acoustic and bathymetry data were acquired in March 2016 onboard R/V Maria
177 S. Merian (see Hübscher et al., 2017). The cruise MSM52 collected ca. 3500 km of MCS data throughout
178 large area from Bay of Kiel to north-east of Bornholm (Hübscher et al., 2017, Hübscher, 2018). Due to
179 some malfunction of the parametric sediment profiler and multibeam echosounder, some of the seismic
180 lines have no coverage of these data. MCS seismic data allowed to investigate salt tectonics in North
181 German Basin (Ahlrich et al., 2020, 2022), explain structural evolution and inversion tectonics along the
182 Tornquist Zone (Krzywiec et al., 2022; Pan et al., 2022).

183 *3.1. Multi-channel reflection seismic data and well data*

184 MCS acquisition was tuned to provide high-resolution data and a gap-less image from the seafloor to deeper
185 subsurface. Toward this end, relatively short minimum offset (37.5 m) and high-frequency air-gun array (8
186 GI guns) was employed. Acquisition parameters are summarized in Table 1.

Parameter	Value
Number of channels	216
Receiver group interval	12.5 m
Average shot interval	25 m
Minimum offset	37.5 m
Maximum offset	2710 m
Streamer tow depth	3 m
Airgun array tow depth	2 m
Airgun array	8 x GI guns (1200 inch ³ total volume)

187 Table 1. Acquisition parameters of MCS data acquired during MSM52 cruise (Hübscher et al., 2017)

188 The MCS dataset used in this study were processed in-house at Institute of Geophysics, Polish Academy of
189 Sciences. Seismic data processing workflow included several demultiple techniques such as SRME, Tau-P
190 deconvolution, water bottom FK filtering (see more details in Nguyen, 2020; Nguyen et al. 2022 in prep).
191 In this study, we use 2 profiles from MSM52 cruise (line BGR16-212 and BGR16-256) (see Figure 1 for
192 location). Final seismic sections were pre-stack time migrated. The stratigraphy horizons were correlated
193 from nearby well K9-1/89, for which time – depth charts (check-shot data) and stratigraphy formation tops
194 were provided (unpublished Petrobaltic report).

195 *3.2. Hydro-acoustics data and bathymetry data*

196 The uppermost sediment layers were surveyed using parametric sediment profiler (PARASOUND DS III-
197 P70 system) from Atlas Hydrographic hull-mounted at R/V Maria S. Merian. By simultaneously emitting
198 two primary frequencies between 19 and 23.5 kHz, a parametric frequency of around 4 kHz is created,
199 allowing for a maximum penetration depth of approximately 200 m beneath the seafloor, although in the
200 area of shallow water the image recorded was clear for interpretation up to a dozen of meters beneath the
201 seafloor (above the multiple). The acquired hydro-acoustic data were processed using MDPS (Meridata,
202 Finland) software.

203 The seafloor morphology was surveyed by a hull-mounted SIMRAD EM122 multibeam echo-sounder
204 system. Multibeam data were processed using QINSY and QIMERA software. The raw data files have been
205 loaded into QIMERA as Processed Point files (QPD). The processing uses a strong spline filter and CUBE
206 processing. In addition, due to the lack of repeated water sound velocity profiles, external beams were
207 rejected and refraction correction was added. Bathymetry grids with regular 0.75 m cell were created for
208 the analyzed profiles.

209 *3.3. Seismic attributes and amplitude versus offset analysis*

210 Seismic attributes are commonly used in seismic interpretation to automate highlighting specific features,
211 often difficult to decipher by human interpreter (Marfurt, 2018). Seismic attributes can help in tracking
212 fluid expulsion (e.g., gas escape features) (Cartwright and Santamarina, 2015) and dissolution or collapse
213 features (e.g., Sullivan et al., 2006; Singh et al., 2016; Meldahl et al., 1999). So-called geometrical attributes
214 (Chopra and Marfurt, 2007), such as the coherence attribute, are commonly used in detection of faults,
215 fractures and chaotic zones.

216 Amplitude versus offset (AVO) can be considered as a specific quantitative seismic interpretation attribute.
217 It is commonly used in the oil and gas exploration industry to identify reservoir zones, fluids and lithologies.
218 The two AVO attributes, AVO Intercept and Gradient, are calculated from pre-stack angle gathers using
219 Aki-Richards 2 term equation (Aki and Richards, 1980), an approximation of full Zoeppritz reflectivity
220 equations (Hilterman, 2001). Intercept is the P-wave reflection coefficient at normal incidence of an event,
221 while gradient represents regression of amplitude variations taken at different angles of incidence (Russell,
222 2002). AVO technique is rarely applied in shallow gas studies because of problems in obtaining sufficient
223 angle coverage at shallow depths, however it can be used to check where the gas distribution on the seismic
224 section and where the gas can migrate to the surface.

225

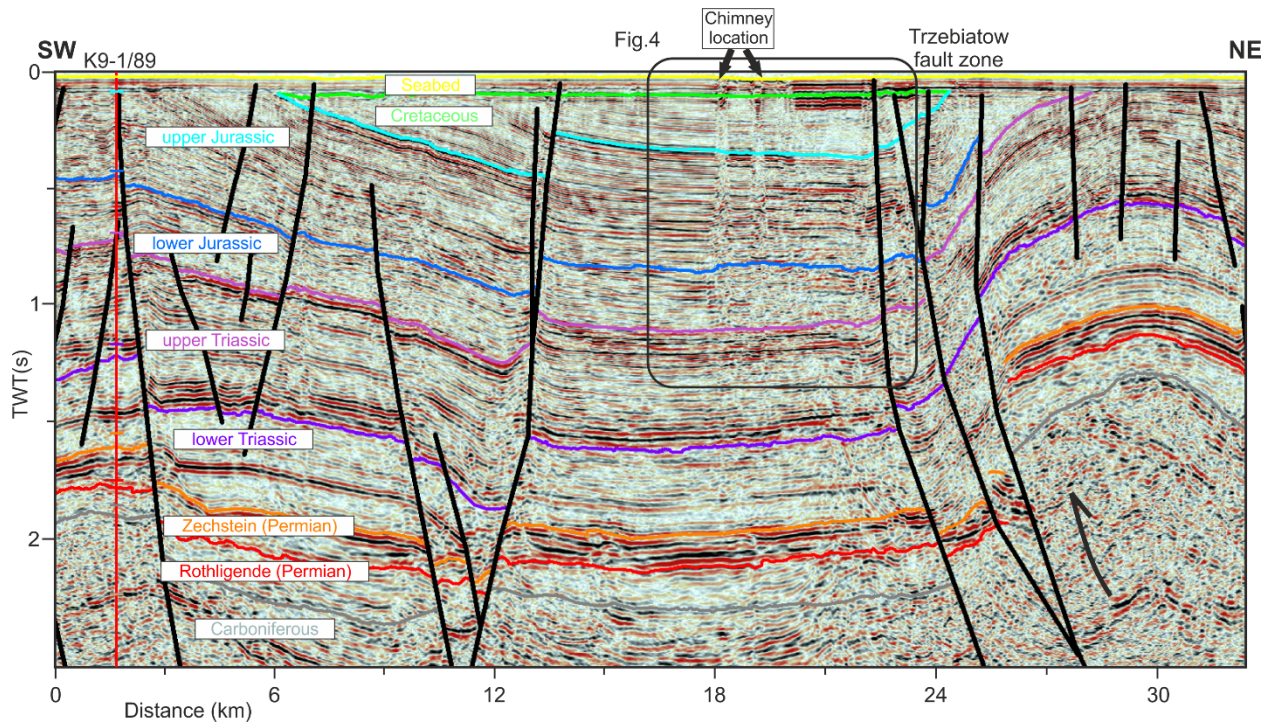
226 **4. Results**

227 Data availability and identified shallow gas features were compiled in Table 2.

Data availability	BGR16-212	BGR16-256	BGR16-257
MCS	yes	yes	yes
Parametric sediment profiler	yes	yes	no
Multibeam	no	yes	yes
Shallow gas observations			
Gas chimneys	yes	yes	-
Pockmarks	-	yes	yes
Shallow geology			
Holocene mud	yes	no	no

228 Table 2. Data availability and shallow gas features in 3 profiles: BGR16-212, BGR16-256 and BGR16-
 229 257.

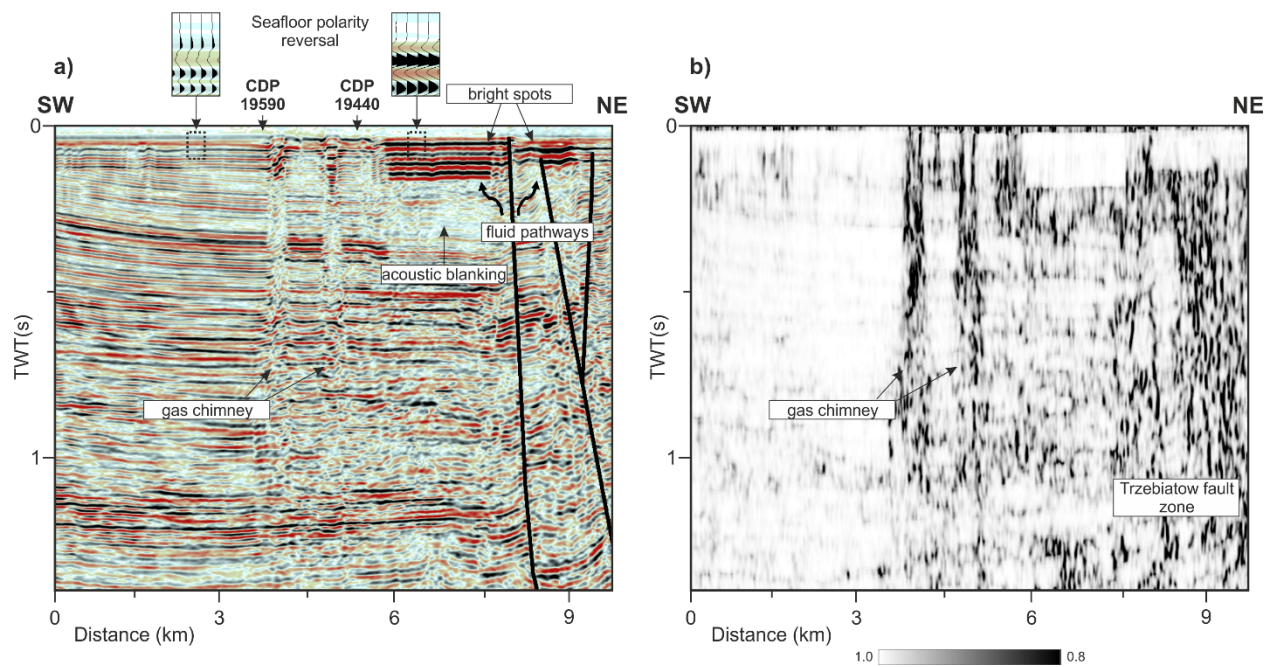
230 *4.1. Line BGR16 – 212*



231
 232 **Figure 3.** Part of the interpreted pre-stack time migrated seismic section along profile BGR16-212 across
 233 well K9-1/89, the Trzebiatów fault zone and the Gryfice block (see Figure 1 for the location of the seismic

234 profile and well). Two gas chimneys were identified near the eastern part of the Gryfice block, closed to
235 the Trzebiatów fault zone. Rectangle marks the area displayed in Figure 4.

236 We start with the structural and stratigraphic interpretation of the seismic section BGR16-212 crossing
237 important geological features such as Adler-Kamien and Trzebiatów faults zone (Figure 3). Interpretation
238 was based on well K9-1/89 stratigraphy markers, unpublished well reports, regional cross sections and
239 previous studies (both offshore and onshore) (Jaworowski et al., 2010; Pokorski, 2010; Krzywiec, 2006).
240 Line BGR16-212 crosses an asymmetric fault-propagation fold and is accompanied by reverse Trzebiatów
241 fault zone in the NE of the section (Figure 3). Due to the strong uplift of inversion anticlines, all Cretaceous
242 and part of Late Mesozoic sediments were eroded. Toward SW of the section, there are few normal faults
243 systems formed during syn-rift basin extensional period. Sediment thicknesses of Mesozoic remain stable
244 in this area. Notice that the Cretaceous formation is significantly eroded due to strong uplift of inversion
245 anticlines, only small amount of 100-300 ms of Upper Cretaceous sediment was left over in the Gryfice
246 block (Figure 3). Two gas chimneys are identified in the section (Figure 4) together with the high amplitude
247 reflections (bright spots) close to the Trzebiatów fault zone.



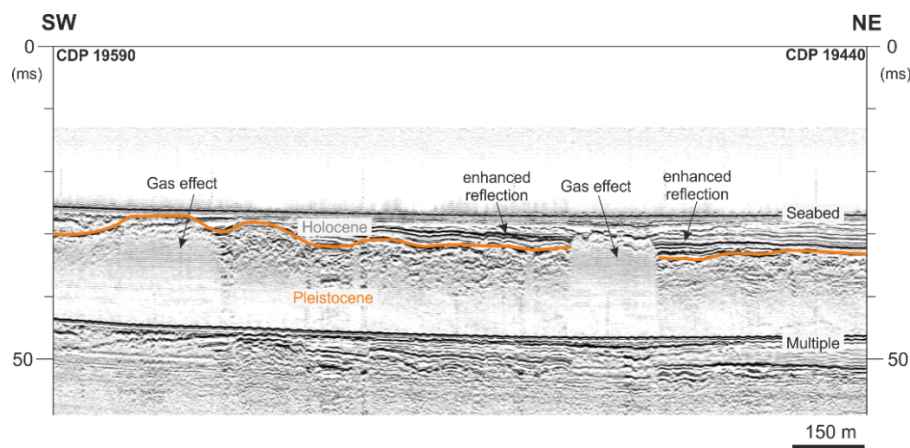
248

249 **Figure 4.** Part of the seismic section BGR16-212 (a) and its coherence attribute section (b). Evidence of
250 shallow gas features is interpreted including gas chimneys, bright spots (enhanced reflection), acoustic
251 blanking and seafloor polarity reversal.

252 Zoom in part of section BGR16-212 provides clearer image of the shallow gas features (Figure 4).
253 Reflectivity of gas chimneys appears as a chaotic zone, with low trace-to-trace coherence and lower
254 amplitudes as compared with adjacent sediments. Taking advantage of this behavior, the coherence seismic
255 attribute was employed to help interpret free gas associated features (Figure 4b). Gas chimneys are more
256 discriminated as high coherence values to continuous events. The Trzebiatów fault zone is also highlighted
257 as noisy area due to discontinuous reflectivity at fault location. More importantly, low coherence zone of
258 the gas columns is much reduced around interval of 1.1 to 1.2 s, which may suggest potential existence of
259 a gas reservoir in the past at this interval.

260 Bright spots are identified on top of the Trzebiatów fault zone (Figure 4a), suggest a potential of free gas
261 migration pathway through the faults to shallow sediments. Reflection of these bright spots shows as peak
262 (positive amplitude), reverse of the seafloor reflection (Figure 4a). Bright spot areas are associated with the
263 reverberations, as the consequence of strong impedance contrast between the layers of gas accumulated
264 shallow sediments (Davy, 1992; Tóth et al., 2014). It is impossible to differentiate these reverberations with
265 the main reflector due to very shallow water environment of the Baltic Sea (~30 ms in this area).

266 Apart from polarity reversal, bright spots and gas chimneys, acoustic blanking zone is identified below the
267 bright spots and reverberations in the seismic section (Figure 4a). In this case, acoustic blanking happened
268 below the bright spots, which indicates attenuation of seismic energy by the gas charged sediments.

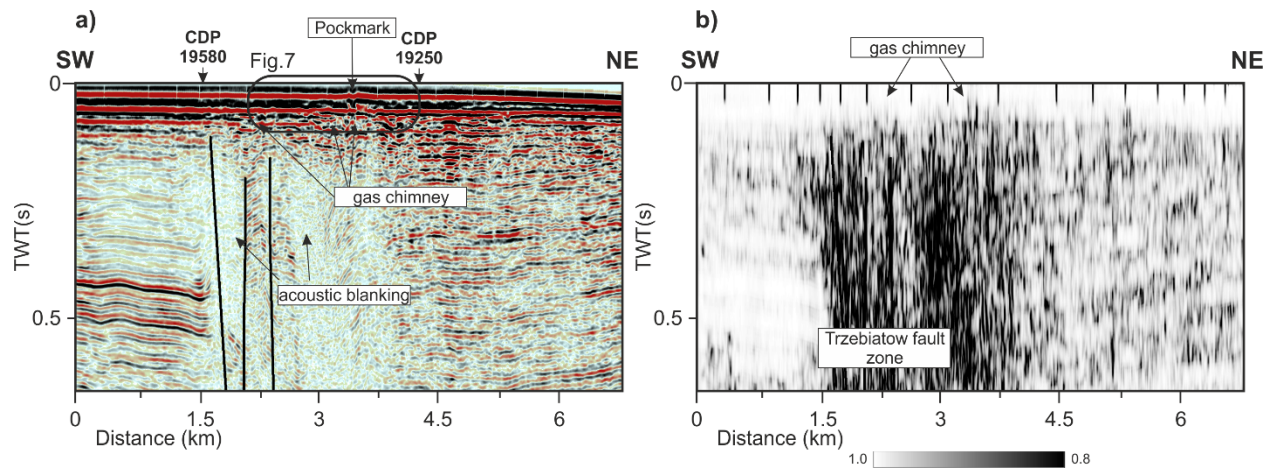


269
270 **Figure 5.** Hydro-acoustic data (parametric sediment profiler) from profile BGR16-212 between CDP 19440
271 to 19590, crossing gas chimneys identified in the MCS data. Boundary between Pleistocene and Holocene
272 sediments (orange) is interpreted in this profile.

273 The gas chimneys identified in seismic data are also associated with the disturbances in amplitude pattern
274 in the parametric sounding data (Figure 5). Gas chimneys are clearly marked within the Pleistocene

275 sediments as non-reflective vertical zones. The width of the two zones identified along the profile is
 276 approximately 150 and 250 m, respectively. Chimneys/anomalous amplitude zones do not reach the sea
 277 bottom - the gas reaches the upper glacial till or is dispersed in the paleolakes' sediment layer. Close to the
 278 gas effect zones, some enhanced reflections are identified (Figure 5), which may prove that the gas is
 279 charged to Holocene sediments instead of leaking to the sea surface. However, such reflections may also
 280 result from the lithological variability (e.g. presence of organic layers, such as pit, gyttja) or/and deposits
 281 structure (e.g., layering/stratification).

282 4.2. Line BGR16 – 256



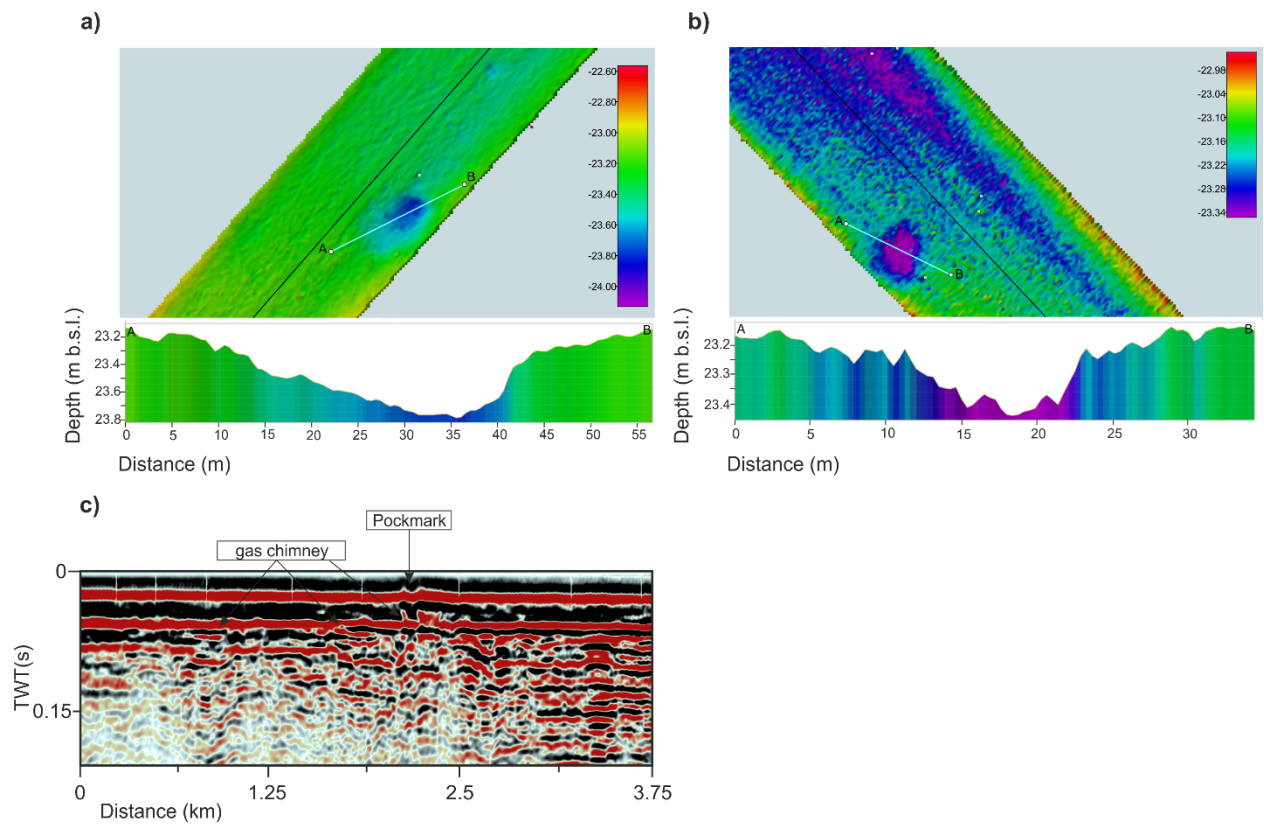
283

284 **Figure 6.** Part of the pre-stack time migrated seismic section along profile BGR16-256 and the
 285 corresponding coherence attribute section (see Figure 1 for the location of seismic profile). Evidence of
 286 shallow gas features is interpreted including gas chimneys, acoustic blanking and pockmarks.

287 Shallow gas expressions were also interpreted along profile BGR16-256 toward the northwest of the
 288 Trzebiatów fault zone. We identified gas chimneys, acoustic blanking and pockmarks in the seismic section
 289 (Figure 6). The columns of gas are much smaller than observed along line BGR16-212. They may only be
 290 recognized by little polarity changes close to the seafloor (Figure 7). The utility of the coherence attribute
 291 section is minimal in this case as locations of these gas columns are close to the complicated Trzebiatów
 292 fault zone. Acoustic blanking zones in this line appear at around 0.2 to 0.5 s joint with the fault zone (Figure
 293 6). The coherence attribute shows a large low value zone which represents huge discontinuity zone due to
 294 faulting, fracturing and presumed free gas activities.

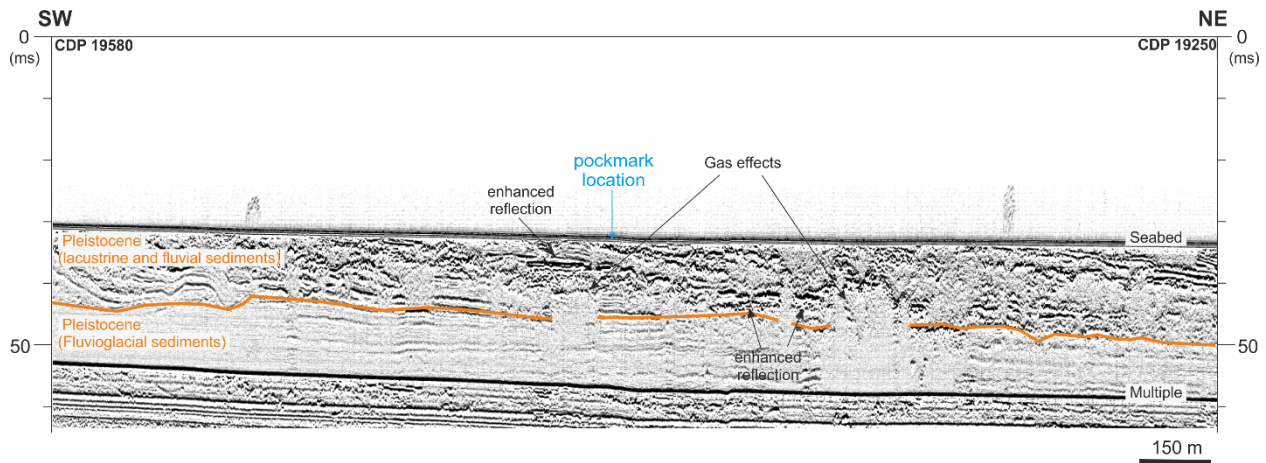
295 The analysis of the bathymetric data along lines BGR16-256 and BGR16-257 (seismic data from the latter
 296 were not interpreted as it follows the strike of the Trzebiatów fault) indicates that in some places the gas
 297 also reaches the seabed, creating small oval depressions (Figure 7). The asymmetric form recorded along

298 line BGR16-256 is about 35 m in diameter and 60 cm deep (Figure 7a). Features identified along line
299 BGR16-257 is smaller, approximately 25 m in diameter and only 20 cm deep (Figure 7b).



300

301 **Figure 7.** Seafloor topography build from multibeam data close to the pockmark identified along line
302 BGR16-256 (a). Seafloor expressions of a pockmark identified at the strike profile (BGR16-257) (b). For
303 position of these pockmarks, see Figure 1. (c) Part of the seismic section profile BGR16-256 at the identified
304 pockmark location.



305

306 **Figure 8.** Hydro-acoustic data (parametric sediment profiler) from profile BGR16-256 between CDP 19250
 307 and 19580, crossing the gas chimneys and pockmark in line BGR16-256. Boundary between 2 types of
 308 Pleistocene sediments (orange) is interpreted whereas Holocene mud sediment is absent in this profile. Note
 309 that the pockmark is not recognized in this hydro-acoustic data.

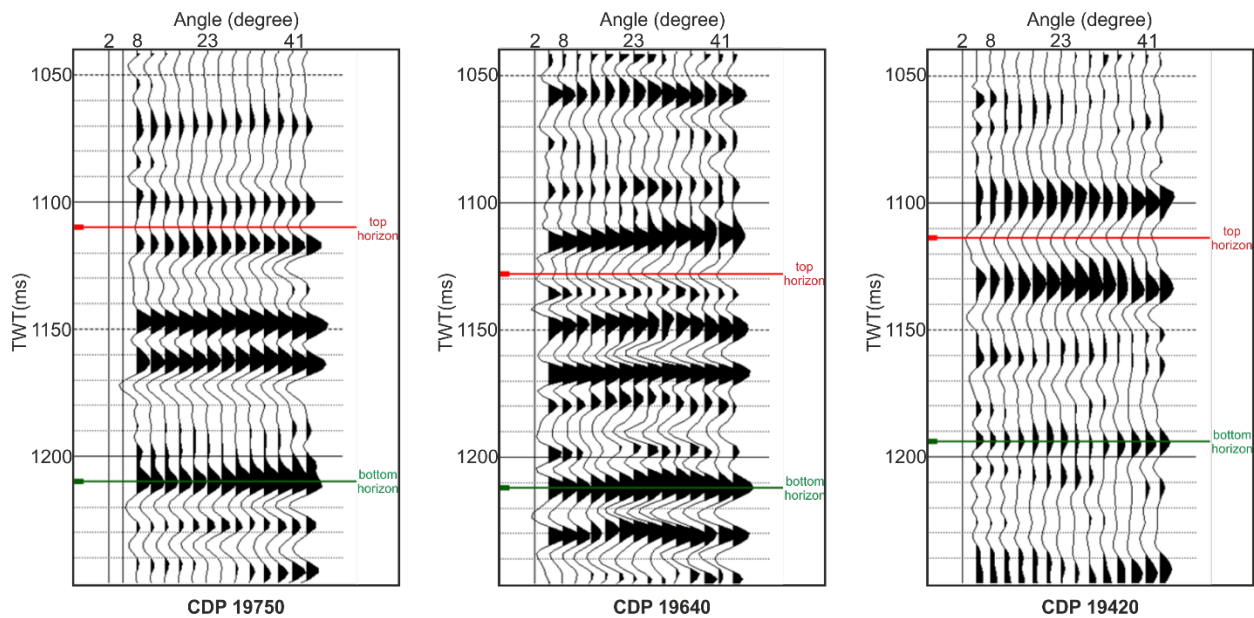
310 Gas chimneys are less pronounced in the parametric sediment profiler data (Figure 8) than in the line
 311 BGR16-212. It is possible that in an environment with a distinct predominance of non-cohesive deposits,
 312 represented here by river and lake sands and silty sands of MIS3, the gas is more easily dispersed inside the
 313 layers of these deposits. Anomalies caused by gas columns are still recognizable. Enhanced reflection
 314 zones, identified surrounding these anomalies probably indicate occurrence of more cohesive inter-layers,
 315 hardly permeable to gas. The structure of these layers is variable and locally the gas reaches sea surface
 316 forming small pockmarks (Figure 7). Toward SW part, the hydro-acoustic data become significantly lower
 317 quality (Figure 8). It can be also caused by shallow gas activity.

318 *4.3. AVO analysis along line BGR16-212*

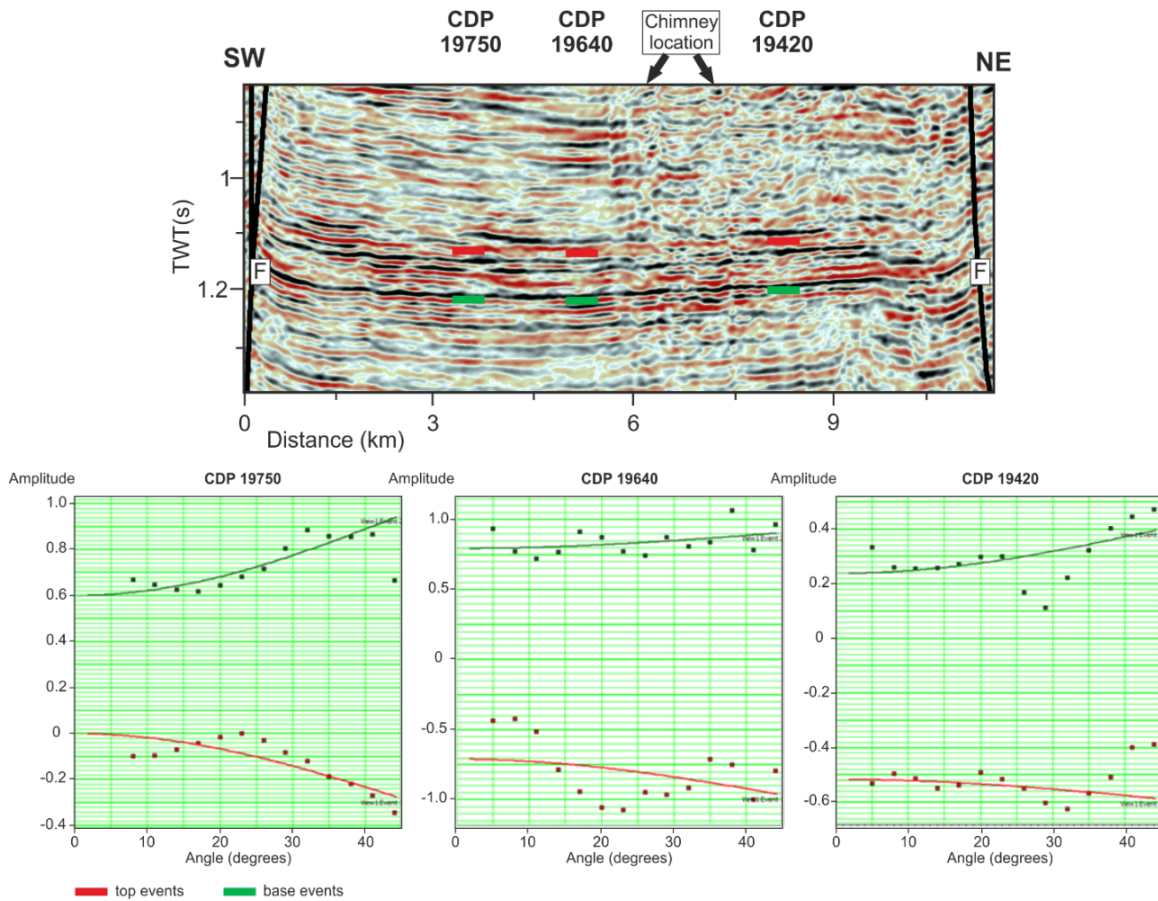
319 In order to prove the existence of free gas remains in the potential reservoir and to discriminate fluid effect
 320 with normal background rock property, we performed AVO analysis. We followed a conventional
 321 workflow of AVO application. First, the CDP gathers are muted to remove traces beyond maximum
 322 incident angle of 45 degrees (angle mute). Signal-to-noise ratio is improved through super gather creation
 323 and residual move-out is eliminated through trim statics. AVO analysis is carried out at the presumed
 324 location of the potential gas accumulation within the Upper Triassic formation (root zone of gas chimneys
 325 identified along line BGR16-212, Figure 4). Target zone of AVO analysis is restricted at the interval of 100
 326 ms (around 1.1 to 1.2 s TWT) and limited between the Trzebiatów Fault and a normal fault in the SW of
 327 the section. Figure 9 shows 3 angle gathers at selected locations surrounding the gas chimneys (CDP

328 numbers 19420, 19640 and 19750) (see location of the CDP gathers in Figure 10). Notice that the three
329 CDP gathers were chosen based on scanning through the whole NMO-corrected CDP gathers of line
330 BGR16-212 as most representative CDP gathers exhibiting AVO effect at the interest interval.

331 The CDP gathers were corrected using processing velocity. Top horizon (red) is marked at ~1.11 s as a top
332 of the reservoir. Bottom horizon (green) is marked at ~1.21 s as a presumed base of the reservoir (Figure
333 9). The top and base of the potential reservoir here was based on enhanced reflections visible in seismic
334 section. They may not represent for true top and base of the gas deposit in the potential reservoir. The AVO
335 Intercept and AVO Gradient were selected from the major trough and peak pair at 3 CDPs (19420, 19640
336 and 19750) (Figure 10). The amplitude variation clearly shows class 2 AVO which has small negative
337 reflection coefficient at zero offset and amplitude increase with offset (Castagna and Swan, 1997) in 3 CDP
338 gathers. This trend indicates presence of remnant free gas in the Upper Triassic reservoir rocks.



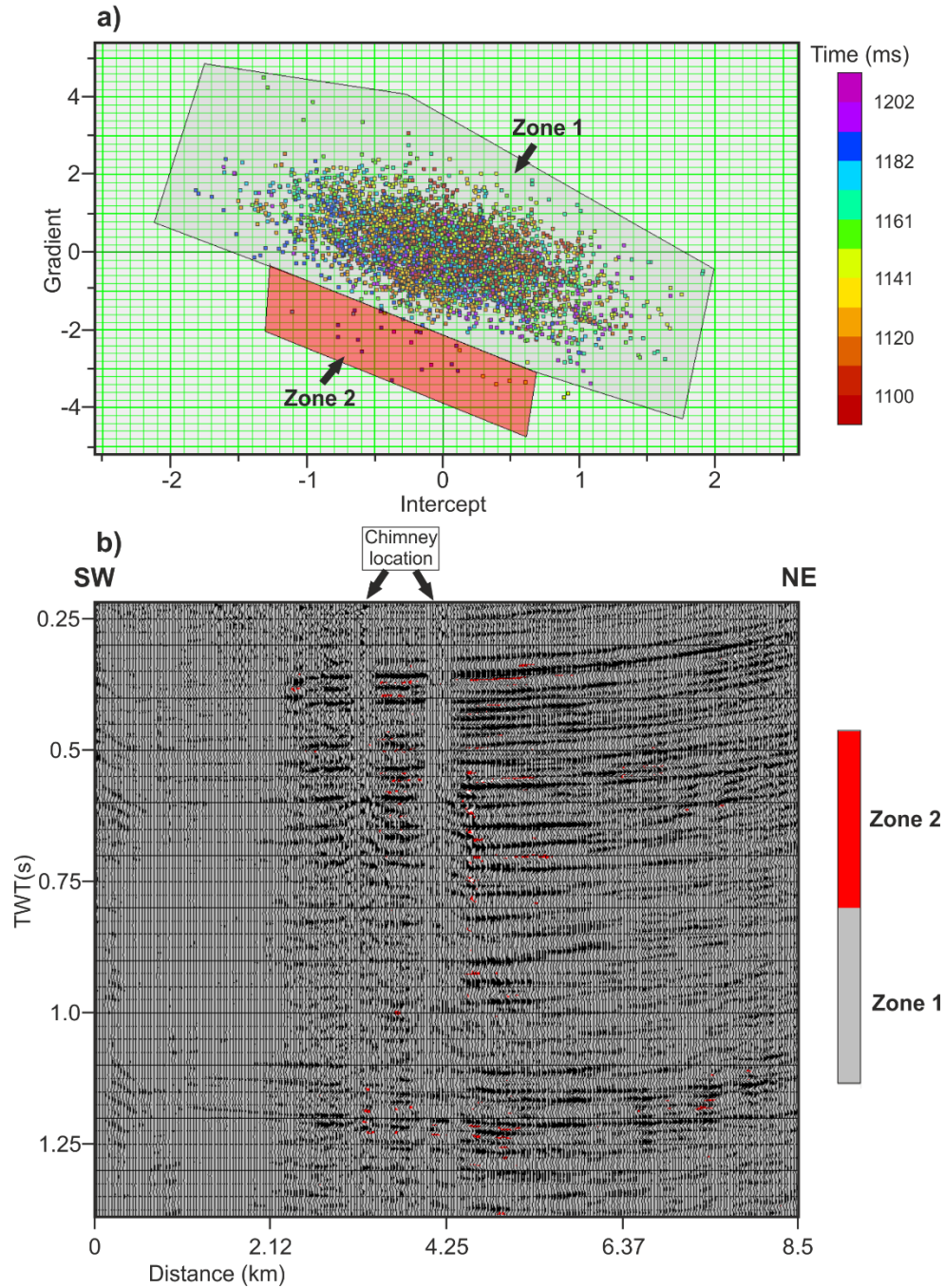
339
340 **Figure 9.** Angle gather extracted from profile BGR16-212, at CDP super gathers 19750, 19640 and 19420.
341 Locations of the CDP points on stack section are shown in Figure 10. Top horizon (red) marks top of the
342 potential reservoir, bottom horizon marks base of the potential reservoir. Normal move-out correction is
343 applied using stacking velocity.



344

345 **Figure 10.** Gradient analysis of the angle gathers shown in Figure 9. Locations of the CDP gathers are
 346 chosen surrounding the chimneys' locations and at the potential reservoir interval (a). (b) Trough (red) and
 347 peak (green) seismic amplitudes are displayed with angle (offsets) at the depth of around 1.15 s TWT for
 348 CDP number 19420, 19640 and 19750.

349 Cross-plot of the derived AVO Intercept/Gradient is presented in Figure 11 to further investigate the type
 350 of AVO anomalies. The expected background trend is delineated as zone 1, while anomalous events were
 351 delineated as zone 2, consistent with class 2 AVO anomalies. Both zones were projected back onto the
 352 seismic section. AVO anomalies interpreted as free gas charged sediments (red color) are highlighted in the
 353 section (Figure 11). Majority of the free gas related anomalies are located within the predicted potential gas
 354 reservoir and along the gas chimneys' pathways.



355

356 **Figure 11.** AVO Intercept/Gradient cross-plot and seismic amplitude and AVO anomaly section along part
 357 of line BGR16-212. (a) Cross-plot shows background trend (grey) (zone 1) and AVO anomaly (red) (zone
 358 2). (b) Zone 1 and 2 mapped on seismic section close to the chimneys' location.

359 **5. Discussion**

360 *5.1. Seismic and hydro-acoustic indicators of shallow gas*

361 Evidence of the free gas in sediments of the Gryfice block are proved by indicative shallow gas features
362 including gas chimneys, seafloor polarity reversal, bright spots, acoustic blanking and pockmarks. Two big
363 gas chimneys interpreted along line BGR16-212 can be tracked down with support of seismic attributes to
364 around 1.1 - 1.2 s TWT. This suggests rooting of these gas chimneys at Upper Triassic formation. The gas
365 chimneys identified in line BGR16-256 (Figure 6) are less distinct and behave more as seepage style, which
366 is “small and localized” (Schroot and Schuttenhelm, 2003). These small gas seepages possibly leak slowly
367 to the surface through tiny holes or gaps caused by faults’ activities. Such structures are visible closer to
368 the Trzebiatów fault zone, indicating an escape path of the free gas from deeper successions to shallow
369 sediments. The free gas possibly begins to migrate during the Late Cretaceous inversion period together
370 with inverted activity of the Trzebiatów fault zone. Gas reaches also Pleistocene and Holocene deposits.
371 Leaking of the gas associated with the pockmarks was registered close to lines BGR16-256/257 (no
372 multibeam data available for line BGR16-212).

373 Apart from indicated gas features, velocity pull-down is a typical feature represented for free gas presence
374 in sediments underneath seafloor. It happens because the compressional wave propagation velocity is
375 decreased below the value for water saturated sediment, attenuation of acoustic waves propagating through
376 gassy sediment and acoustic reflection and/or scattering are increased (Anderson and Bryant, 1990).
377 Problem of imaging artifacts in form of pull-downs is contrasted with the pull-ups concept caused by high-
378 velocity localized anomaly (e.g., till within tunnel valleys; Frahm et al., 2020). Structural image below the
379 gas charged shallow sediments could be misinterpreted as localized syncline-like features. Some of these
380 features are visible in the gas chimney area in line BGR16-212 (Figure 4), however the far- and near-offset
381 stacks, as well as the general appearance of the reflectivity inside the chimney, suggest that it is not caused
382 by dimming of the reflections due to the shallow gas anomaly only. What we observe in the seismic data is
383 probably a combination of those two effects: shallow low-velocity anomaly and extensive fluid (gas) escape
384 route.

385 Geochemical analysis also proves that the Trzebiatów fault zone is active in term of migration process and
386 seepage of liquid and gaseous hydrocarbon (Jaworowski et al., 2010). The most liquid hydrocarbon seepage
387 into bottom waters crosses the axial of the fault zone, while high methane concentration in water is observed
388 in the southern part of the fault zone (Wagner, 2011). Migration of the gaseous and liquid hydrocarbons
389 occurs despite the occurrence of sealing Zechstein salts. These geogenic substances can originate from the
390 beneath Devonian, Carboniferous, Zechstein Main Dolomite source rock. Therefore, the Trzebiatów fault
391 zone and western part of the Kolobrzeg Block represent a high geogenic pollution risk (Jaworowski et al.,
392 2010).

393 Two anomalies at the gas chimneys' locations are clearly identified in the hydro-acoustic data along line
394 BGR16-212 (Figure 5). They are characterized by small scattering points on top of the free gas and
395 especially acoustic blanking behaviors below the gas charged layer. This acoustic blanking represents of
396 low reflection and interruption image of the below sediment layer due to presence of free gas (Toth et al.,
397 2014). It also appears that the gas columns did not reach the water bottom and stop within
398 Holocene/Pleistocene sediments boundary. It is possible that after migrating from the below successions,
399 the free gas did not escape through sea bed but might accumulate to very shallow sediments (Pleistocene –
400 early Holocene). This hypothesis is further reinforced by the presence of bright spots close to the gas
401 columns as well as polarity reversals of the seabed reflectors. Besides, in the seismic section, these high-
402 amplitude reflectors cause heavy reverberations below the water bottom (Toth et al., 2014). Enhanced
403 reflection in layer deposited within Holocene formation may indicate occurrence of more cohesive, hardly
404 permeable to gas internal layers, where the gas accumulates. This parasound image is similar to gas
405 accumulation structures in Holocene marine mud that were recorded in Bay of Aarhus (Jensen and Bennike,
406 2009), Bornholm Basin (Laier and Jensen, 2007; Toth et al., 2014) and other sedimentation basins of the
407 Southern Baltic Sea (e.g., Jaśniewicz et al., 2019; Idczak, et al., 2020).

408 Gas effects are more obscure along line BGR16-256 (Figure 8), what most probably result from different
409 lithological formations of Quaternary deposits in this area (Kramarska, 1998). 2 types of Pleistocene
410 sediments can be differentiated by high amplitude, chaos reflection of lacustrine and fluvial origins
411 sediments, compared to dim and flat reflection of fluvio-glacial origin sediments. Anomalies caused by gas
412 activities can be identified by scattering points and blanking zones within the fluvio-glacial related sands
413 and river and lake related fine-grained sands. These sands could possibly be potential deposits of the free
414 gas in Pleistocene sediments. The pockmarks identified by multibeam data (Figure 7) and enhanced
415 reflection features identified surrounding the gas effects illustrates simultaneous free gas accumulation and
416 sea surface leakage.

417 The coherence seismic attribute, commonly used to detect discontinuities (faults, fractures), seems to be an
418 effective tool to detect and differentiate free gas associated features from other seismic events in the section
419 (Figure 4 and 6). Due to absorption and scattering of the seismic energy, chaotic behavior of seismic signal
420 of the gas chimneys and acoustic blanking can be differentiated compared to continuous seismic events of
421 adjacent areas within the section. Attribute section enabled to delineate the rooting point of the gas
422 chimneys along line BGR16-212 (Figure 4). The attribute anomalies of the columns start from around 1.2
423 s TWT. It suggests an upward pathway for the free gas to migrate from Upper Triassic formation to shallow
424 formations. The Trzebiatów fault zone appears as a mixture of coherence anomalies due to discontinuity of
425 seismic events within a complex faults zone. For profile BGR16-256 (Figure 6), the anomalies caused by

426 gas or faulting are difficult to be differentiated as location of small gas chimneys are too close to the
427 Trzebiatów fault zone. However, this may prove that the gas migrates from much deeper to shallow
428 sediments and then to surface through the faults system.

429 *5.2. AVO attribute analysis*

430 After interpreting the indicators of shallow gas in seismic section, a starting point of the gas chimneys in
431 line BGR16-212 is recognized by the coherence seismic attributes. It reveals a possibility of a potential gas
432 reservoir existence at around 1.1 to 1.2 s TWT, in the Upper Triassic formation, so there is a high chance
433 there are still free gas remains in this interval. Due to limited of lithology information and lack of well data,
434 to verify this hypothesis, AVO analysis was only used to detect the remnant of free gas in the potential
435 reservoir.

436 Accumulation of gas in rocks causes decrease in velocity and density, as the results there will be decrease
437 in acoustic impedance (AI) of the formation (Simm and Bacon, 2014). The angle gathers of line BGR16-
438 212 shows the increase of amplitudes in far offsets which represents for the decrease of AI due to free gas
439 presence (Figure 9). AVO class 2 anomalies from the angle gathers were identified by gradient analysis
440 plots as near zero impedance contrast between charged gas sand and surrounding non-gas sand and shale
441 (mudstones). The class 2 AVO illustrates the similar properties of mudstones and gas sands at the presumed
442 reservoirs interval and nature of the sand is compacted and consolidated. This matches with lithology of
443 the Triassic and Jurassic formations in the Gryfice block dominantly composing of interbedded sands and
444 mudstones with very thin carbonate and evaporates layers (Figure 2). It might be concluded that the free
445 gas could not be trapped permanently at the potential reservoirs due to homogenous of lithology between
446 Mesozoic sediments and absence of good overlying seal.

447 Using the scatter plot of intercept against gradient (Figure 11a), the low negative gradient represents for
448 contained gas rock (zone 2, red) was discriminated from the background trend of surrounding normal rock
449 property (zone 1, grey). Therefore, samples with no AVO behavior in grey polygon (zone 1) could imply
450 for this dominant interbedded sand and mudstones, while it is not possible to conclude precisely the type
451 of sand that contains the free gas in red zone (zone 2) due to lack of nearby well data information. So in
452 this study, we just call it contained gas sand. The free gas was exactly highlighted in the section, not only
453 at the potential reservoir interval (1.1 – 1.2 s TWT) but also in whole Upper Triassic – Jurassic formation.
454 Deposition of the free gas proves the hypothesis of origin of the gas chimneys and free gas “crept” to
455 sediment layers throughout the gas chimneys migration pathways.

456 AVO technique was rarely applied in other fields than petroleum exploration, especially for shallow gas
457 study. Kim et al., (2020) was possibly the only study that included AVO analysis for identifying free gas,
458 helping to discriminate water contacts and bright events among the chaotic signals on the MCS data. Our
459 study is probably the first one in which shallow gas can be linked with a potential deeper gas reservoir via
460 AVO analysis.

461 *5.3. Petroleum system and shallow gas expressions*

462 Linking of shallow gas to near surface sediments was carried out in several investigations in nearby areas
463 of the offshore West Pomerania, Southern Baltic Sea. Connections of geological settings of near surface
464 sediments with distribution of methane were showed in Eckernförde Bay (Abegg and Anderson, 1997) and
465 in Aarhus Bay (Jensen and Bennike, 2009). In Arkona Basin, characterization of acoustic turbidity caused
466 by gas presence in near surface sediments were investigated by geochemical, core analysis and very high-
467 resolution seismic profiles (Mathys et al. 2005, Thieben et al. 2006). In Bornholm Basin, Tóth et al. (2014)
468 linked free shallow gas with organic-rich Holocene marine mud by velocity field analysis in MCS data.
469 Further north and east of Gotland Basin, Schäfer et al. (2021) interpreted phase reversed seismic reflections
470 beneath the Quaternary Klints Bank drumlin as evidence for hydrocarbon gas accumulation of thermogenic
471 origin.

472 In this study, the shallow gas expressions from seismic and hydroacoustic data illustrate a leaking
473 hydrocarbon play offshore West Pomerania. The free gas probably generates initially from the source rocks
474 in Palaeozoic and Permian (Carboniferous mudstones and Main Dolomite Zechstein) (Kotarba et al., 2008;
475 Karnkowski et al., 2010). The free gas then escapes to upper sediments through either the Trzebiatów fault
476 zone or directly in areas where the Zechstein evaporates are thin or absent. This is more likely to happen
477 when dominant sediments of Lower to Middle Triassic compose of just interbedded sand and mudstones
478 layers. The Keuper (Middle - Upper Triassic) formation comprises of various types of potential reservoir
479 rocks: fine grain sandstone and carbonate evaporates. In addition, the oil and gas prone window of the West
480 Pomeranian falls into this period (Kosakowski et al., 2006; Karnkowski et al., 2010). Therefore, there are
481 favorable conditions that the free gas can charge these rocks. Moreover, AVO analysis at the potential
482 reservoir interval also proves the presence of remnant free gas in the Upper Triassic formation.

483 Based on the seismic interpretation, seismic attributes and lithology of the study area, there are two possible
484 migration pathways of the free gas from the potential reservoir in the Upper Triassic sediments to seabed:
485 through gas columns and through reactivated (during Late Cretaceous inversion) Trzebiatów fault zone.
486 The first pathway can be explained that there is no good seal layer on top of the Upper Triassic, and free
487 gas could creep through unconsolidated successions above to near surface. The second pathway can be due

488 to strong reactivation of the existing listric faults, which created spaces for free gas to escape to the shallow
489 sediments.

490 **6. Conclusions**

491 Shallow gas-escape related features were for the first time identified in the seismic and hydro-acoustic data
492 in Pomeranian Bight, offshore western Poland. Various indicators of gas features including seismic
493 chimneys, bright spots, acoustic blanking were interpreted on seismic sections with support of seismic
494 attributes. In the area of dominance of near-bottom Quaternary sandy sediments the gas can leak to the
495 seabed, forming small (25-35 m diameter) pockmarks. Those shallow gas features were linked with the
496 activity of the Trzebiatów fault zone. We hypothesize that this fault zone is providing potential fluid
497 pathways of the free gas from Carboniferous or Zechstein formation “kitchen” below to migrate to Upper
498 Triassic sediments or directly to Quaternary shallow sediments. This hypothesis was also supported from
499 geochemical data from some previous studies. Some evidences from the parametric sediment profiler data
500 suggest that after migration, the free gas either accumulates in near surface Quaternary sediments or is
501 leaking to the seafloor.

502 The use of AVO analysis technique in shallow gas investigation is highlighted in this study. AVO attributes
503 analysis proves the presence of remnant free gas in the potential Upper Triassic reservoir (at ~1.15-1.2 s),
504 which supports hypothesis of gas reservoir existence in the past and origin of free gas escape to shallow
505 sediments.

506 Our study also proves the potential of hydrocarbon existence in the offshore West Pomerania, which is still
507 considered as poor hydrocarbon exploration area in the Polish territorial waters.

508 **Acknowledgements**

509 This study was funded by the Polish National Science Centre grant no UMO-2017/27/B/ST10/02316.
510 Cruise MSM52 has been funded by German Science Foundation DFG and Federal Ministry of Education
511 and Research (BMBF). We thank Federal Institute for Geosciences and Natural Resources (BGR) for the
512 license to use seismic data acquired during MSM52 cruise and their support during seismic data acquisition.

513 We would like to thank IHS Markit Ltd. and GeoSoftware for the donation of academic licenses of Kingdom
514 Suite and Hampson Rusell software packages. Seismic data processing was performed using Globe Claritas
515 package under the academic license from Petrosys Ltd.

516 **Data availability**

517 Data are uploaded to PANGAEA database and will be released after acceptance of the manuscript. Web
518 link and DOI will be updated during the revision process.

519 **Author contribution statement**

520 **Quang Nguyen:** Conceptualization, Methodology, Data Curation, Writing – Original Draft preparation,
521 Software, Visualization. **Michal Malinowski:** Supervision, Project administration, Writing – Review &
522 Editing. **Regina Kramarska** and **Dorota Kaulbarsz:** Data Curation, Writing – Original Draft preparation.
523 **Leslaw Mil:** Data Curation. **Christian Hübscher:** Project administration, Funding acquisition, Writing –
524 Review.

525 **Declaration of competing interest**

526 The author declare that they have no known competing financial interests or personal relationships that
527 could have appeared to influence the work reported in this paper.

528 **References**

529 Abegg, F. and Anderson, A.L., 1997. The acoustic turbid layer in muddy sediments of Eckernförde Bay,
530 Western Baltic: methane concentration, saturation and bubble characteristics. *Marine Geology*, 137(1-2),
531 pp.137-147.

532 Adams, N.J. and Kuhlman, L.G., 1991, November. Shallow gas blowout kill operations. In *Middle East Oil*
533 *Show*. OnePetro.

534 Ahlrichs, N., Hübscher, C., Noack, V., Schnabel, M., Damm, V. and Krawczyk, C.M., 2020. Structural
535 evolution at the northeast North German Basin margin: From initial Triassic salt movement to Late
536 Cretaceous-Cenozoic remobilization. *Tectonics*, 39(7), p.e2019TC005927.

537 Ahlrichs, N., Noack, V., Hübscher, C., Seidel, E., Warwel, A. and Kley, J., 2022. Impact of Late Cretaceous
538 inversion and Cenozoic extension on salt structure growth in the Baltic sector of the North German Basin.
539 *Basin Research*, 34(1), pp.220-250.

540 Aki, K. and Richards, P.G., 1980. *Quantitative seismology, theory and methods*, Vol. 1 WH Freeman &
541 Co. New York.

542 Anderson, A.L. and Bryant, W.R., 1990. Gassy sediment occurrence and properties: Northern Gulf of
543 Mexico. *Geo-Marine Letters*, 10, pp.209-220.

544 Bachmann, G.H. and Geluk, M.C., 2010. Chapter 9, Triassic. *Petroleum Geological Atlas of the Southern*
545 *Permian Basin Area*. EAGE Publications BV, Houten, 148, p.173.

- 546 Brodecka, A., Majewski, P., Bolałek, J. and Klusek, Z., 2013. Geochemical and acoustic evidence for the
547 occurrence of methane in sediments of the Polish sector of the southern Baltic Sea. *Oceanologia*, 55(4),
548 pp.951-978.
- 549 Cartwright, J. and Santamarina, C., 2015. Seismic characteristics of fluid escape pipes in sedimentary
550 basins: implications for pipe genesis. *Marine and Petroleum Geology*, 65, pp.126-140.
- 551 Castagna, J.P. and Swan, H.W., 1997. Principles of AVO crossplotting. *The leading edge*, 16(4), pp.337-
552 344.
- 553 Chopra, S. and Marfurt, K.J., 2007. Seismic attributes for prospect identification and reservoir
554 characterization. Society of Exploration Geophysicists and European Association of Geoscientists and
555 Engineers.
- 556 Dadlez, R., 1978. Podpermskie kompleksy skalne w strefie Koszalin–Chojnice. *Geological Quarterly*,
557 22(2), pp.269-302.
- 558 Dadlez, R., 1980. Tektonika wału pomorskiego. *Geological Quarterly*, 24(4).
- 559 Dadlez, R., Narkiewicz, M., Stephenson, R.A., Visser, M.T.M. and Van Wees, J.D., 1995. Tectonic
560 evolution of the Mid-Polish Trough: modelling implications and significance for central European geology.
561 *Tectonophysics*, 252(1-4), pp.179-195.
- 562 Dadlez, J., 2002. Cyclic sedimentation in the Middle Jurassic of central Poland. *Geological Quarterly*,
563 46(3), pp.321-335.
- 564 Dadlez, R., 2003. Mesozoic thickness pattern in the Mid-Polish Trough. *Geological Quarterly*, 47, pp.223-
565 240.
- 566 Davy, B., 1992. Seismic reflection profiling on southern lake rotorua-evidence for gas-charged lakefloor
567 sediments. *Geothermics*, 21(1-2), pp.97-108.
- 568 Erlström, M., Thomas, S.A., Deeks, N. and Sivhed, U., 1997. Structure and tectonic evolution of the
569 Tornquist Zone and adjacent sedimentary basins in Scania and the southern Baltic Sea area.
570 *Tectonophysics*, 271(3-4), pp.191-215.
- 571 Fleischer, P., Orsi, T., Richardson, M. and Anderson, A., 2001. Distribution of free gas in marine sediments:
572 a global overview. *Geo-Marine Letters*, 21(2), pp.103-122.
- 573 Floodgate, G.D. and Judd, A.G., 1992. The origins of shallow gas. *Continental shelf research*, 12(10),
574 pp.1145-1156.
- 575 Frahm, L., Hübscher, C., Warwel, A., Preine, J. and Huster, H., 2020. Misinterpretation of velocity pull-
576 ups caused by high-velocity infill of tunnel valleys in the southern Baltic Sea. *Near Surface Geophysics*,
577 18(6), pp.643-657.
- 578 Frick, M., Kranz, S., Norden, B., Bruhn, D. and Fuchs, S., 2022. Geothermal Resources and ATEs Potential
579 of Mesozoic Reservoirs in the North German Basin. *Energies*, 15(6), p.1980.

- 580 Garcia-Gil, S., Vilas, F. and Garcia-Garcia, A., 2002. Shallow gas features in incised-valley fills (Ria de
581 Vigo, NW Spain): a case study. *Continental Shelf Research*, 22(16), pp.2303-2315.
- 582 Gawenda, P., 2011. Germany–Overview about Renewed Petroleum Activities. AAPG-European Region
583 Newsletter, pp.4-9.
- 584 Hilterman, F.J., 2001. Seismic amplitude interpretation. Society of Exploration Geophysicists and
585 European Association of Geoscientists and Engineers.
- 586 Hovland, M. and Judd, A.G., 1988. Seabed pockmarks and seepages: impact on geology, biology and the
587 marine environment (Vol. 293). London: Graham & Trotman.
- 588 Hovland, M., Judd, A.G. and Burke Jr, R.A., 1993. The global flux of methane from shallow submarine
589 sediments. *Chemosphere*, 26(1-4), pp.559-578.
- 590 Hübscher, C., Ahlrichs, H., Allum, G., Behrens, T., Bülow, J., Krawczyk, C., Damm, V., Demir, Ü., Engels,
591 M., Frahm, L. and Grzyb, G., 2017. BalTec-Cruise No. MSM52–March 1–March 28, 2016–Rostock
592 (Germany)–Kiel (Germany). MARIA S. MERIAN-Berichte, MSM52, 46 pp., DFG-Senatskommission für
593 Ozeanographie.
- 594 Hübscher, Christian (2018): Geophysical profiles during Maria S. Merian cruise MSM52. Institut für
595 Geophysik, Universität Hamburg, PANGAEA, <https://doi.org/10.1594/PANGAEA.890870>
- 596 Idczak, J., Brodecka-Goluch, A., Łukawska-Matuszewska, K., Graca, B., Gorska, N., Klusek, Z., Pezacki,
597 P.D. and Bolałek, J., 2020. A geophysical, geochemical and microbiological study of a newly discovered
598 pockmark with active gas seepage and submarine groundwater discharge (MET1-BH, central Gulf of
599 Gdańsk, southern Baltic Sea). *Science of The Total Environment*, 742, p.140306.
- 600 Jakacki, J., Klusek, Z., Têgowski, J. and Warszawy, P., 2002. The non-linear method of gas bubbles
601 detection in the bottom sediments. *Revista de Acustica*, 33.
- 602 Janik, T., Wójcik, D., Ponikowska, M., Mazur, S., Skrzynik, T., Malinowski, M. and Hübscher, C., 2022.
603 Crustal structure across the Teisseyre-Tornquist Zone offshore Poland based on a new refraction/wide-
604 angle reflection profile and potential field modelling. *Tectonophysics*, 828, p.229271.
- 605 Jaśniewicz, D., Klusek, Z., Brodecka-Goluch, A. and Bolałek, J., 2019. Acoustic investigations of shallow
606 gas in the southern Baltic Sea (Polish Exclusive Economic Zone): a review. *Geo-Marine Letters*, 39(1),
607 pp.1-17.
- 608 Jaworowski, K., Wagner, R., Modliski, Z., Pokorski, J., Sokołowski, J. and Sokołowski, A., 2010. Marine
609 ecogeology in semi-closed basin: case study on a threat of geogenic pollution of the southern Baltic Sea
610 (Polish Exclusive Economic Zone). *Geological Quarterly*, 54(2), pp.267-288.
- 611 Jensen, J.B. and Bennike, O., 2009. Geological setting as background for methane distribution in Holocene
612 mud deposits, Århus Bay, Denmark. *Continental Shelf Research*, 29(5-6), pp.775-784.

- 613 Jørgensen, B.B., and Fossing, H., 2012. Methane gas and seismo-acoustic mapping, in: Jørgensen, B.B,
614 Fossing, H., (Eds.), Baltic Gas final scientific report. pp 8-12.
- 615 Judd, A.G. and Hovland, M., 1992. The evidence of shallow gas in marine sediments. *Continental Shelf*
616 *Research*, 12(10), pp.1081-1095.
- 617 Judd, A. and Hovland, M., 2009. *Seabed fluid flow: the impact on geology, biology and the marine*
618 *environment*. Cambridge University Press.
- 619 Karnkowski, P. H., Pikulski, L. and Wolnowski, T., 2010. Petroleum geology of the Polish part of the Baltic
620 region - an overview. *Geological Quarterly*, 54 (2), pp.143–158.
- 621 Kilhams, B., Kukla, P.A., Mazur, S., McKie, T., Mijnlieff, H.F. and van Ojik, K. eds., 2018, August.
622 Mesozoic resource potential in the Southern Permian Basin. Geological Society of London.
- 623 Kim, Y.J., Cheong, S., Chun, J.H., Cukur, D., Kim, S.P., Kim, J.K. and Kim, B.Y., 2020. Identification of
624 shallow gas by seismic data and AVO processing: Example from the southwestern continental shelf of the
625 Ulleung Basin, East Sea, Korea. *Marine and Petroleum Geology*, 117, p.104346.
- 626 Kosakowski, P., Kotarba, M.J., Pokorski, J. and Wróbel, M., 2006, June. Hydrocarbon potential of the
627 Carboniferous strata on the Kołobrzeg and Gryfice blocks (Northwestern Poland). In 68th EAGE
628 Conference and Exhibition incorporating SPE EUROPEC 2006 (pp. cp-2). European Association of
629 Geoscientists & Engineers.
- 630 Kotarba, M.J., Kosakowski, P., Więclaw, D., Grelowski, C., Kowalski, A., Lech, S. and Merta, H., 2004.
631 Potencjał węglowodorowy karbońskich skał macierzystych w przybałtyckiej części segmentu pomorskiego
632 bruzdy śródpolskiej. *Przegląd Geologiczny*, 52(12), pp.1156-1165.
- 633 Kramarska, R., 1998. Origin and development of the Odra Bank in the light of the geologic structure and
634 radiocarbon dating. *Kwartalnik Geologiczny*, 42(3), pp.277-288.
- 635 Kramarska, R., Krzywiec, P., Dadlez, R., Jegliński, W., Papiernik, B., Przedziecki, P. and Zientara, P.,
636 1999. Geological map of the Baltic Sea bottom without Quaternary deposits, 1:500 000. Państw. Inst. Geol.,
637 Gdańsk-Warszawa.
- 638 Kraus, J., Rott, C., and Damte, A., 2018. Tectonic Evolution and Hydrocarbon Exploration of a Multiple
639 Overprinted Caledonian Continental Collision Zone in the German Baltic Sea. *Search and Discovery*
640 *Article #11064 (2018)*.
- 641 Krzywiec, P., 2002. The Oświno structure (NW Mid-Polish Trough)-salt diapir or inversion-related
642 compressional structure?. *Geological Quarterly*, 46, pp.337-346.
- 643 Krzywiec, P., Kramarska, R. and Zientara, P., 2003. Strike-slip tectonics within the SW Baltic Sea and its
644 relationship to the inversion of the Mid-Polish Trough—evidence from high-resolution seismic data.
645 *Tectonophysics*, 373(1-4), pp.93-105.
- 646 Krzywiec, P., 2006. Structural inversion of the Pomeranian and Kuiavian segments of the Mid-Polish
647 Trough--lateral variations in timing and structural style. *Geological Quarterly*, 50(1), pp.151-168.

648 Krzywiec, P., Stachowska, A., Grzybowski, L., Nguyen, Q., Słonka, L., Malinowski, M., Kramarska, R.,
649 Ahlrichs, N., Hübscher, C., 2022. The Late Cretaceous inversion of the Polish Basin and surrounding area
650 – a current perspective based on seismic data, In book: Cretaceous of Poland and of adjacent areas. Field
651 trip guides. 11th International Cretaceous Symposium, Warsaw, Poland. Publisher: Faculty of Geology,
652 University of Warsaw.

653 Laier, T. and Jensen, J.B., 2007. Shallow gas depth-contour map of the Skagerrak-western Baltic Sea
654 region. *Geo-Marine Letters*, 27(2), pp.127-141.

655 Majewski, P. and Klusek, Z., 2011. Expressions of shallow gas in the Gdansk Basin. *Zeszyty naukowe*
656 *Akademii Marynarki Wojennej*, 52, pp.61-71.

657 Majewski, P. and Klusek, Z., 2014. Parameters of echo signals originated from a gas seepage site in the
658 southern Baltic Sea. *Hydroacoustics*, 17, pp.143–150.

659 Marfurt, K.J., Kirlin, R.L., Farmer, S.L. and Bahorich, M.S., 1998. 3-D seismic attributes using a
660 semblance-based coherency algorithm. *Geophysics*, 63(4), pp.1150-1165.

661 Marfurt, K.J., 2018. Seismic attributes as the framework for data integration throughout the oilfield life
662 cycle. Society of Exploration Geophysicists.

663 Mathys, M., Thiessen, O., Theilen, F., Schmidt, M., 2005. Seismic characterization of gas-rich near surface
664 sediments in the Arkona Basin, Baltic Sea. *Marine Geophysical Researches*, 26, pp.207–224.

665 Meldahl, P., Heggland, R., Bril, B. and de Groot, P., 1999. The chimney cube, an example of semi-
666 automated detection of seismic objects by directive attributes and neural networks: Part I; methodology. In
667 SEG Technical Program Expanded Abstracts 1999 (pp. 931-934). Society of Exploration Geophysicists.

668 Naudts, L., De Batist, M., Greinert, J. and Artemov, Y., 2009. Geo-and hydro-acoustic manifestations of
669 shallow gas and gas seeps in the Dnepr paleodelta, northwestern Black Sea. *The Leading Edge*, 28(9),
670 pp.1030-1040.

671 Nguyen Q, 2020, Seismic Data Processing Report (BALTEC / MSM52). Institute of Geophysics PAS.
672 <https://dspace.igf.edu.pl/xmlui/handle/123456789/112>.

673 Pan, Y., Seidel, E., Juhlin, C., Hübscher, C. and Sopher, D., 2022. Inversion tectonics in the Sorgenfrei–
674 Tornquist Zone: insight from new marine seismic data at the Bornholm Gat, SW Baltic Sea. *GFF*, 144(2),
675 pp.71-88.

676 Parkes, R.J., Cragg, B.A., Fry, J.C., Herbert, R.A. and Wimpenny, J.W.T., 1990. Bacterial biomass and activity
677 in deep sediment layers from the Peru margin. *Philosophical Transactions of the Royal Society of London. Series*
678 *A, Mathematical and Physical Sciences*, 331(1616), pp.139-153.

679 Pernille-1 unpublished well report, 1989.

680 Pokorski, J., 2010. Geological section through the lower Paleozoic strata of the Polish part of the Baltic
681 region. *Geological Quarterly*, 54(2), pp.123-130.

- 682 Ren, S., Liu, Y., Huang, F. and Zhang, P., 2019. Quantitative Classification of Shallow Gas Blowout during
683 Offshore Drilling Process. *Journal of Petroleum & Environmental Biotechnology*, 10(393), pp.1-6.
- 684 Russell, B.H., Lines, L.R. and Ross, C.P., 2002. AVO classification using neural networks: A comparison
685 of two methods. *CREWES Res. Rep.*, 14, pp.1-18.
- 686 Schäfer, W., Hübscher, C., Sopher, D., 2021. Seismic stratigraphy of the Klints Bank east of Gotland (Baltic
687 Sea): A giant drumlin sealing thermogenic hydrocarbons. *Geo-Marine Letters* 41:9,
688 doi.org/10.1007/s00367-020-00683-3.
- 689 Scheck-Wenderoth, M. and Lamarche, J., 2005. Crustal memory and basin evolution in the Central
690 European Basin System—new insights from a 3D structural model. *Tectonophysics*, 397(1-2), pp.143-165.
- 691 Schlüter, H.U., Best, G., Jürgens, U. and Binot, F., 1997. Interpretation reflexionsseismischer Profile
692 zwischen baltischer Kontinentalplatte und kaledonischem Becken in der südlichen Ostsee-erste Ergebnisse.
693 *Zeitschrift der deutschen geologischen Gesellschaft*, pp.1-32.
- 694 Schroot, B.M. and Schüttenhelm, R.T., 2003. Shallow gas and gas seepage: expressions on seismic and
695 other acoustic data from the Netherlands North Sea. *Journal of Geochemical Exploration*, 78, pp.305-309.
- 696 Schroot, B.M. and Schüttenhelm, R.T.E., 2003. Expressions of shallow gas in the Netherlands North Sea.
697 *Netherlands Journal of Geosciences*, 82(1), pp.91-105.
- 698 Schroot, B.M., Klaver, G.T. and Schüttenhelm, R.T., 2005. Surface and subsurface expressions of gas
699 seepage to the seabed—examples from the Southern North Sea. *Marine and Petroleum Geology*, 22(4),
700 pp.499-515.
- 701 Simm, R., Bacon, M. and Bacon, M., 2014. *Seismic amplitude: An interpreter's handbook*. Cambridge
702 University Press.
- 703 Singh, D., Kumar, P.C. and Sain, K., 2016. Interpretation of gas chimney from seismic data using artificial
704 neural network: A study from Maari 3D prospect in the Taranaki basin, New Zealand. *Journal of Natural
705 Gas Science and Engineering*, 36, pp.339-357.
- 706 Stina-1 unpublished well report, 1989.
- 707 Sullivan, E.C., Marfurt, K.J., Lacazette, A. and Ammerman, M., 2006. Application of new seismic
708 attributes to collapse chimneys in the Fort Worth Basin. *Geophysics*, 71(4), pp.B111-B119.
- 709 Tęgowski, J., Jakacki, J., Klusek, Z., Rudowski, S., 2003. Nonlinear acoustical methods in the detection of
710 gassy sediments in the Gulf of Gdańsk. *Hydroacoustics*, 6, pp.151–158.
- 711 Thießen, O., Schmidt, M., Theilen, F., Schmitt, M. and Klein, G., 2006. Methane formation and distribution
712 of acoustic turbidity in organic-rich surface sediments in the Arkona Basin, Baltic Sea. *Continental Shelf
713 Research*, 26(19), pp.2469-2483.
- 714 Tóth, Z., Spieß, V. and Jensen, J., 2014. Seismo-acoustic signatures of shallow free gas in the Bornholm
715 Basin, Baltic Sea. *Continental Shelf Research*, 88, pp.228-239.

- 716 Tóth, Z., Spiess, V. and Keil, H., 2015. Frequency dependence in seismoacoustic imaging of shallow free
717 gas due to gas bubble resonance. *Journal of geophysical research: solid earth*, 120(12), pp.8056-8072.
- 718 Vejbaek, O.V., Stouge, S. and Damtoft Poulsen, K., 1994. Palaeozoic tectonic and sedimentary evolution
719 and hydrocarbon prospectivity in the Bornholm area.
- 720 Wagner, R., 2011. Natural migration of liquid and gaseous subsurface hydrocarbons into bottom sediments
721 and waters. In: Uścińowicz, S. (Ed.), *Geochemistry of Baltic Sea surface sediments*. Polish Geological
722 Institute - National Research Institute, Warsaw, pp. 125–145.
- 723 Zimmermann, J., Franz, M., Heunisch, C., Luppold, F.W., Mönnig, E. and Wolfgramm, M., 2015. Sequence
724 stratigraphic framework of the Lower and Middle Jurassic in the North German Basin: Epicontinental
725 sequences controlled by Boreal cycles. *Palaeogeography, Palaeoclimatology, Palaeoecology*, 440, pp.395-
726 416.
- 727
- 728